The effect of engine spin direction on the dynamics of powered two wheelers

To appear in *Vehicle System Dynamics*
Vol. 00, No. 00, Month 20XX, 1–16

The effect of engine spin direction on the dynamics of powered two wheelers

Matteo Massaro* and Edoardo Marconi

Department of Industrial Engineering, University of Padova, Via Venezia 1, 35131 Padova, Italy

(*Received 00 Month 20XX; accepted 00 Month 20XX*)

The effect of engine spin direction on the dynamics of powered two wheelers is investigated in terms of steady state points (equilibria), vibration modes (stability), manoeuvre time (performance/manoeuvrability) and handling. The goal is to assess and quantify the advantage sometimes claimed for the 'counter-rotating' engine configuration, where the engine spins in the opposite direction with respect to wheels, against the 'conventional' configuration, where the engine spins in the same direction of wheels.

Keywords: powered two wheelers (PTW); motorcycles; engine; spin direction; weave and wobble; minimum manoeuvre time.

1. Introduction

Some race motorcycles are equipped with the so-called 'counter-rotating' engine, where counter-rotating refers to the spin direction of the engine crankshaft with respect to the spin direction of wheels. Indeed, the 'conventional' configuration for transverse engine motorcycles is with the engine crankshaft spinning in the same direction of wheels. This standard configuration is usually chosen for simplicity of constructions. In a basic configuration the crankshaft (spin rate $+\omega_e$) engages with the gearbox primary shaft (spin rate $-\omega_p$), which in turn engages with the gearbox secondary shaft (spin rate $+\omega_s$), where the chain sprocket is also mounted [1]. The rear wheel (spin rate $+\omega_r$) clearly rotates in the same direction of the chain sprocket due to the chain transmission.

It is well known that counter-rotating configurations are deemed advantageous is some scenarios, although these scenarios have never been stated clearly and the related advantages (if any) quantified. The objective of the current work is to asses the differences between the conventional and counter-rotating layouts in a number of typical conditions. Such conditions have been selected after the analysis of the basics of motorcycle dynamics. The engine spin direction affects the vehicle angular momentum. The angular momentum and its variation affect the load transfer in acceleration/braking and the gyroscopic moments.

Steady turning is analysed in order to evaluate the effect of the two configurations on the vehicle trim, namely on the equilibrium roll angle. Eigenvalue analysis is performed in order to evaluate the effect of engine configuration on vibration modes, namely on weave

*Corresponding author. Email: matteo.massaro@unipd.it

and wobble. Limit acceleration and limit braking manoeuvres are analysed in order to asses the effect of spin direction on the vehicle performance. Lane change manoeuvres are simulated in order to estimate the effect of the engine configuration on handling.

While steady-state and stability analyses are somehow standard, limit acceleration/deceleration simulations are not, since they usually require some form of controller to mimic the rider's behaviour [2–6]. Assuming to have such rider controller, one may wonder whether results are related to the specific and predefined controller structure. To avoid this issue, we employ nonlinear optimal control techniques, where no pre-defined controller structure needs to be chosen. Examples of application related to minimum time manoeuvring of cars and motorcycle are reported in the literature [7–11].

The work is organized as follows. In section 2 the basic effects related to engine spin direction are summarized, in section 3 the key features of the vehicle model employed in this work are revised, while in section 4, 5, 6 and 7 the results related to steady state, stability, acceleration/deceleration performance and handling are discussed.

2. Basics

This section will summarize the main effects of engine spin direction on motorcycle dynamics. Simple formulae will be given when available.

The horizontal, vertical and pitch (with respect to the point A in Fig. 1) equilibria of a motorcycle are

$$ma_x = F_{xf} + F_{xr} - F_d \tag{1}$$

$$0 = N_f + N_r - mg \tag{2}$$

$$I_{wf}\dot{\omega}_f + I_{wf}\dot{\omega}_r \pm I_e\dot{\omega}_e = N_r b - N_f\,(w-b) - (F_{xf}+F_{xr})\,h - F_d\,(h_a - h)\,. \tag{3}$$

In these formulae m is the mass of the whole vehicle and rider, a_x is the longitudinal acceleration, F_{xf} and F_{xr} are the longitudinal forces on the front and rear axles respectively, F_d is the aerodynamic drag force, N_f and N_r are the normal forces on the front and rear tyres respectively, g is the gravity, I_{wf} and I_{wr} are the front- and rear-axle spin moments of inertia, $\dot{\omega}_f$ and $\dot{\omega}_r$ are the front- and rear-axle angular accelerations, I_e is the engine spin moment of inertia[1], $\dot{\omega}_e$ is the engine's spin acceleration, b and h are the horizontal distance and height of the centre of mass from the rear contact point, h_a is the height of the aerodynamic centre and w is the wheelbase. The front and rear vertical loads N_f and N_r can be obtained from (1)-(3)

$$N_f = mg\frac{b}{w} - ma_x\frac{h}{w} - F_d\frac{h_a}{w} - \frac{I_{wf}}{w}\dot{\omega}_f - \frac{I_{wr}}{w}\dot{\omega}_r \mp \frac{I_e}{w}\dot{\omega}_e \tag{4}$$

$$N_r = mg\frac{w-b}{w} + ma_x\frac{h}{w} + F_d\frac{h_a}{w} + \frac{I_{wf}}{w}\dot{\omega}_f + \frac{I_{wr}}{w}\dot{\omega}_r \pm \frac{I_e}{w}\dot{\omega}_e. \tag{5}$$

The first three terms in the N_f and N_r expressions represent the well known terms related to the static vertical loads, the load transfers due to the longitudinal acceleration a_x and the load transfer related to the drag force F_d, while the last three terms are load transfer terms related to the wheel and engine spin inertias. These latter terms are

[1]The engine spin axis is assumed parallel to the wheel axes. A positive sign is used when the engine spin direction is the same as that of the wheels.

usually neglected in classical treatments of the topic, because they are much smaller than the others. However, the latter of these terms is precisely the term related to the effect of engine spin direction and shows that a counter-rotating engine configuration results in a reduced load transfer for a given longitudinal acceleration a_x. Therefore the engine spin direction can potentially affect the acceleration performance of the vehicle.

The engine spin direction also affects the vehicle gyroscopic moments. Indeed wheels, which are the main source of gyroscopic terms, generate gyroscopic moments whenever their main spin velocities $\omega_{r,f}$ combine with some yaw velocity $\dot{\psi}$ or roll velocity $\dot{\phi}$, i.e. whenever the motion differs from a 'perfect' straight motion – perfect means without oscillations. Indeed vibrations around the straight-running equilibrium would generate some yaw and/or roll velocity and thus gyroscopic moments. The engine can be considered as an additional wheel, rotating at a certain speed (which depends on the engaged gear ratio) either in the same direction or opposite direction with respect to the wheels, and thus either increasing or reducing the vehicle gyroscopic moment. In steady turning, each wheel is rotating both around its main spin axis with angular velocity $\omega_{r,f}$ ($\approx V/R_{r,f}$, where V is the vehicle speed and $R_{r,f}$ is the rolling radius of the rear or front wheel) and around the curve centre with yaw angular velocity $\dot{\psi}$. The related gyroscopic moment M_g can be expressed as follows [1]

$$M_g \approx I_{wr,f}\omega_{r,f}\dot{\psi}\cos\phi, \tag{6}$$

where $I_{wr,f}$ is the wheel spin moments of inertia and ϕ is the roll angle. There exists an analogous term for the engine: in this case the engine spin inertia I_e replaces the wheel spin inertia $I_{wr,f}$ and the engine spin velocity ω_e replaces the wheel spin velocity $\omega_{r,f}$. It can be shown [1] that, because of the engine gyroscopic moment, the equilibrium roll angle ϕ of the motorcycle increases by

$$\Delta\phi \approx \frac{I_e\omega_e\dot{\psi}\cos\phi}{h\sqrt{(mg)^2+(ma_y)^2}}, \tag{7}$$

where a_y is the lateral acceleration of the vehicle, and the variation $\Delta\phi$ is with respect to the ideal roll angle $\phi_0 = \arctan(a_y/g)$, possibly corrected for the effect of finite width tyres, which amounts to $\Delta\phi_0 = \arcsin\frac{t\sin\phi_0}{h-t}$, where t is the tyre crown radius. It is worth noting that the inertia I_e in (7) should be introduced with the negative sign in the case of counter-rotating engine.

Finally, the steering effort applied by the rider on the handlebar will have to balance some of the gyroscopic moments acting on the vehicle. It is therefore expected that, although the related effects cannot be predicted with a compact analytical formula, the configuration with the counter-rotating engine would require (slightly) reduced effort when compared with the conventional configuration.

The simulations reported in the following sections 4-7 aim to quantify, using a detailed full vehicle model, the effects suggested by basic principles.

3. Vehicle model

The main features of the motorcycle model to be used in the numerical analysis of sections 4-7 will now be described. The model consists of five bodies (main chassis with a rigidly attached rider, front frame, front wheel, rear wheel and engine) and nine degrees

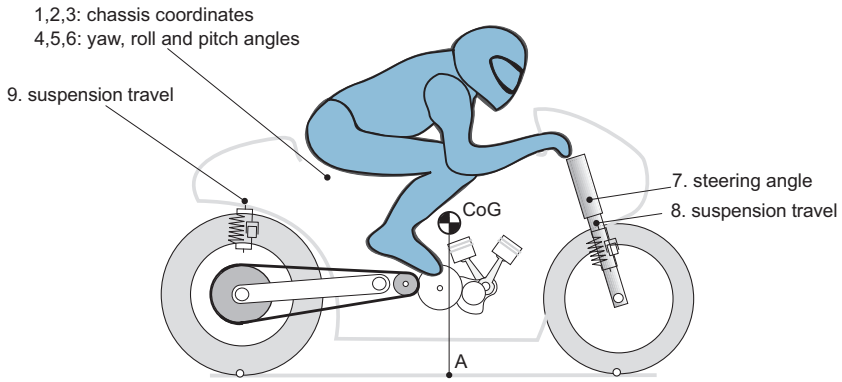

Figure 1.: Motorcycle multibody model with eight degree-of-freedom.

of freedom (chassis position and orientation, steering angle, suspension travels); Fig. 1. The point A in Fig. 1 is defined as the projection of the centre of mass on ground along the vehicle's plane of symmetry. The engine rotation ω_e is related to the rear wheel rotation ω_r through the final drive transmission ratio τ_f, the gearbox ratio τ_g and the primary ratio τ_p, namely

$$\omega_e = \tau_p \tau_g \tau_f \omega_r. \tag{8}$$

For simplicity, the upper chain run is assumed in tension when accelerating while the chain is assumed slack when braking. The tyre model takes into account the shape of the crown radius (assumed toroidal). Steady state lateral forces F_y^0 depend on the slip angle λ and the camber angle ϕ in a linear fashion

$$F_{yr}^0 = (k_{\phi r}\phi_r + k_{\lambda r}\lambda_r)N_r, \tag{9}$$

$$F_{yf}^0 = (k_{\phi f}\phi_f + k_{\lambda f}\lambda_f)N_f, \tag{10}$$

where N_r and N_f are the rear and front tyre normal loads, $k_{\phi r,f}$ and $k_{\lambda r,f}$ are the camber and sideslip stiffness respectively. Relaxation equations are included to account for the well known 'lag' [12] in the generation of tyre forces

$$\frac{\sigma_r}{V_r}\dot{F}_{yr} + F_{yr} = F_{yr}^0, \tag{11}$$

$$\frac{\sigma_f}{V_f}\dot{F}_{yf} + F_{yf} = F_{yf}^0, \tag{12}$$

where σ_r and σ_f are the rear and front tyre relaxation lengths, V_r and V_f are rear and front tyre contact point longitudinal velocity. Pure rolling in the longitudinal direction is assumed. The coupling between lateral and longitudinal forces is accounted using friction ellipses [1]

$$\frac{(\frac{F_{xr}}{\mu_{xr}})^2 + (\frac{F_{yr}}{\mu_{yr}})^2}{N_r^2} \leq 1, \tag{13}$$

$$\frac{(\frac{F_{xf}}{\mu_{xf}})^2 + (\frac{F_{yf}}{\mu_{yf}})^2}{N_f^2} \leq 1, \tag{14}$$

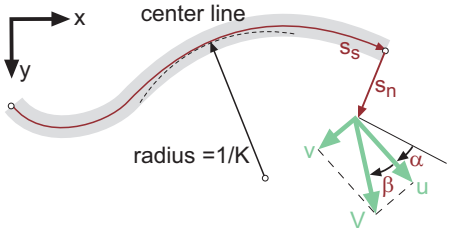

Figure 2.: Vehicle position on the road based on curvilinear coordinates.

where μ_x and μ_y are the friction coefficients in the longitudinal and lateral direction respectively.

The resulting model can be written as a set of 20 first order implicit differential equations

$$\boldsymbol{f}(\boldsymbol{x}, \dot{\boldsymbol{x}}, \boldsymbol{u}) = \boldsymbol{0}. \tag{15}$$

The equations are not reported herein because they are long and complex and can be derived with standard multibody techniques [13, 14]. The corresponding state vector is

$$\boldsymbol{x} = \left\{ V_x, V_y, \dot{\psi}, z, \dot{z}, \phi, \dot{\phi}, \mu, \dot{\mu}, \delta, \dot{\delta}, z_r, \dot{z}_r, z_f, \dot{z}_f, F_{yr}, F_{yf}, s_s, s_n, \alpha \right\}^T, \tag{16}$$

where V_x and V_y are the longitudinal and lateral velocity of the centre of mass, $\dot{\psi}$ is the yaw rate, z is the vertical displacement of the centre of mass, ϕ is the roll angle, μ is the pitch angle, δ is the steering angle, z_r and z_f are the travels of rear and front suspensions respectively, F_{yr} and F_{yf} are the tyres' lateral forces, s_s is the longitudinal position of the vehicle along the track, s_n is the lateral displacement of the vehicle with respect to the centre line of the road and α is the angle between the motorcycle's plane of symmetry and the tangent to the road's centre line; Fig. 2. While the first fifteen state variables in (16) are related to the equations of motion, the sixteenth and seventeenth (F_{yr} and F_{yf}) are related to the relaxation equations (11) and (12), while the last three variables (s_s, s_n and α) are associated to the vehicle position on the road shown in Fig. 2

$$\dot{s}_s = \frac{V\cos(\alpha+\beta)}{1-s_nK}, \tag{17}$$

$$\dot{s}_n = V\sin(\alpha+\beta), \tag{18}$$

$$\dot{\alpha} = \dot{\psi} - K\frac{V\cos(\alpha+\beta)}{1-s_nK}, \tag{19}$$

where $V = \sqrt{u^2+v^2}$ is the velocity of point A in Fig. 1, $\beta = \arctan(v/u)$ is the vehicle sideslip angle at point A and K is the road curvature.

The input vector is

$$\boldsymbol{u} = \{T_h, F_{xr}, F_{xf}\}^T, \tag{20}$$

where T_h is the handlebar steering torque, F_{xr} and F_{xf} are the rear and front tyre longitudinal forces respectively.

The vehicle dataset used in this study is reported in the Appendix.

4. Steady state turning

This section will explain how the steady state analysis is carried out and quantify the effect of engine configuration in steady turning conditions.

The set of differential equations of motion (15) is transformed in a set of algebraic equations when introducing $\dot{V}_x = \dot{V}_y = \dot{z} = \dot{\phi} = \dot{\mu} = \dot{\delta} = \dot{z}_r = \dot{z}_f = 0$. The resulting equations are then solved together with two motion constraints $\sqrt{u^2 + v^2} = V$ and $\dot{\psi}V = a_y$, where the absolute velocity V (at point A in Fig. 1) and the lateral acceleration a_y are given. Therefore the set of algebraic equations can be written as

$$\boldsymbol{f}_s(\boldsymbol{x}_s, \boldsymbol{u}_s) = \boldsymbol{0}, \tag{21}$$

where

$$\boldsymbol{x}_s = \left\{V_x, V_y, \dot{\psi}, z, \phi, \mu, \delta, z_r, z_f, F_{yr}, F_{yf}\right\}^T \qquad \boldsymbol{u}_s = \{T_h, F_{xr}, F_{xf}\}^T \tag{22}$$

which can be solved using a root finding algorithm.

Steady state numerical simulations have been carried out to inspect the effect of engine rotation on the vehicle equilibria for speeds in the range 36-324 km/h (10-90 m/s). The 'optimal' gear ratio is engaged, i.e. the gear ratio that provides the maximum torque at the given speed. The effect of the direction of the engine rotation on the equilibrium roll angle is reported in Fig. 3a, for a lateral acceleration of $10\,\mathrm{m/s^2}$. The stepped behaviour of the the roll angle is explained as follows. The gyroscopic moment (6) goes with $\dot{\psi}\omega$ and thus remains constant when varying speed at constant lateral acceleration, since $a_y = \dot{\psi}V \approx \dot{\psi}\omega/R$. When changing the gear ratio, there is a change in the engine inertia I_e reduced at the rear wheel, in particular the inertia reduces as taller gear ratios are engaged.

The differences between the two configurations (conventional vs. counter-rotating) are minimal, since the gyroscopic moments related to wheels spin are larger than the gyroscopic moment related to the engine spin. Application of (6) at $10\,\mathrm{m/s^2}$ gives 14 Nm for the rear wheel gyroscopic moment, 9 Nm for the front wheel gyroscopic moment and 3.5-1.9 Nm for the engine gyroscopic moment in first and sixth gear respectively.

The wheel gyroscopic moment is related to the vehicle speed, while the engine gyroscopic moment is related to the engine rpm, which depends on the selected gear ratio. Therefore at low speeds and high engine rpm the maximum differences are expected. The numerical results show that the roll angle of the counter-rotating layout is lower by 0.1–0.2 deg when compared with the conventional layout. The behaviour is confirmed by the simplified expression in (7), which predicts the roll angle difference between the conventional and the counter-rotating configuration reported in Fig. 3b.

5. Stability: weave & wobble

The effect of engine configuration on the stability of motorcycles will now be investigated and quantified through eigenvalue analysis.

The vehicle vibration modes hands-off the handlebar are computed as follows. As a first step, the equilibrium (steady state) configuration $\boldsymbol{x}_0, \boldsymbol{u}_0$ is computed with the approach described in Sec. 4. As a second step, the differential equations are linearized around the

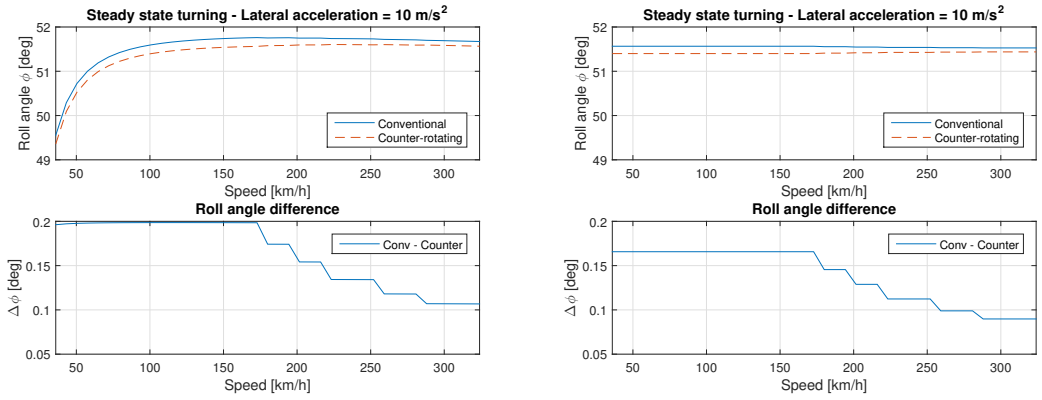

(a) (b)

Figure 3.: Roll angle as a function of speed for conventional and counter-rotating engine: a) simulation results; b) approximated results ($\phi_0 + \Delta\phi_0 + \Delta\phi$).

steady state equilibrium to give the standard state space formulation

$$\Delta\dot{\boldsymbol{x}} = A\Delta\boldsymbol{x} + B\Delta\boldsymbol{u}, \tag{23}$$

where $\Delta\boldsymbol{x} = \boldsymbol{x} - \boldsymbol{x}_0$ and $\Delta\boldsymbol{u} = \boldsymbol{u} - \boldsymbol{u}_0$. Finally, the vibration modes are computed as the eigenvalues of the state matrix A in (23).

The vibration modes of the motorcycle for speeds in the range 10-90 m/s are reported in Fig. 4. Again the 'optimal' gear ratio is selected, i.e. the gear ratio providing the maximum torque at the given speed. The well known weave and wobble are clearly visible and have frequency in the range 0-5 Hz and 6-10 Hz respectively. The in-plane vibration modes are also visible: bounce and pitch have frequencies of 2.5 Hz and 4.5 Hz, while rear-hop and front-hop have frequencies of 8.5 Hz and 16.0 Hz respectively. As usual, in-plane modes in straight motion are almost speed independent [1].

The main effect of the counter-rotating engine configuration is that it slightly reduces the weave stability (Fig. 5a), while the effect on wobble is almost negligible. A similar de-stabilizing effect on weave is obtained when reducing the rear wheel spin inertia, as shown in Fig. 5b, where the rear wheel spin has been varied in the range $\pm 20\,\%$. This confirms that the engine layout effect on stability is mainly related to gyroscopic terms.

6. Performance: acceleration & braking

This section will explain how the effect of engine configuration on the performance of motorcycles is quantified. The analysis of acceleration and braking manoeuvres will follow.

Minimum manoeuvre time simulations have been performed to assess the maximum performance of the vehicle (manoeuvrability) with the two alternative engine layouts. A nonlinear optimal control approach has been employed in order to obtain the solution. The problem consists in finding the optimal controls and optimal states that drive the vehicle from the initial to the final configuration. Therefore there is a cost function, which consists of the manoeuvre time, to be minimized subject to a number of equality and inequality constraints. The equality constraints consists of the equations of motion (15)

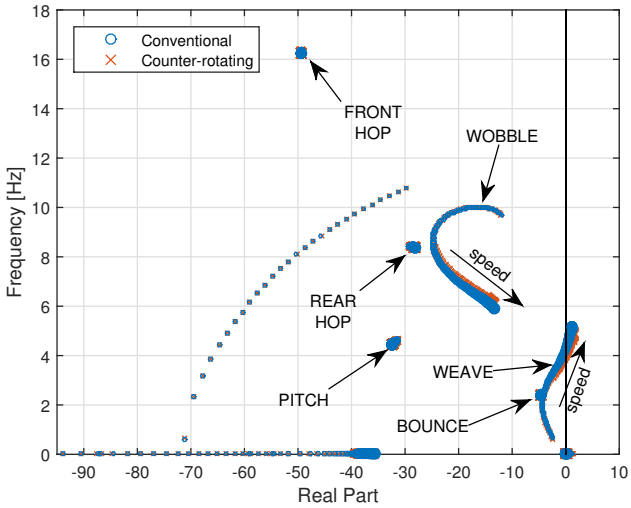

Figure 4.: Vibration modes for conventional and counter-rotating engine for speeds in the range 36-324 km/h (10-90 m/s). Marker size increases with speed.

while the inequality constraints consist of the limitation of the engine power

$$P \leq P_{\max}, \tag{24}$$

the limitation of the steering angle

$$|\delta| \leq \delta_{\max}, \tag{25}$$

the limitation of the maximum steering torque that the rider can apply

$$|T_h| \leq T_{\max}, \tag{26}$$

the maximum tyre friction (friction ellipse)

$$\frac{(\frac{F_{xr}}{\mu_{xr}})^2 + (\frac{F_{yr}}{\mu_{yr}})^2}{N_r^2} \leq 1, \tag{27}$$

$$\frac{(\frac{F_{xf}}{\mu_{xf}})^2 + (\frac{F_{yf}}{\mu_{yf}})^2}{N_f^2} \leq 1, \tag{28}$$

the road borders

$$|s_n| \leq n_{\max}, \tag{29}$$

and the minimum vertical load on tyres

$$N_r \geq 0 \qquad N_f \geq 0. \tag{30}$$

Similarly to [8, 9, 15] the constrained problem is transformed in an equivalent unconstrained problem using Lagrange multipliers and penalty/barrier functions. From the

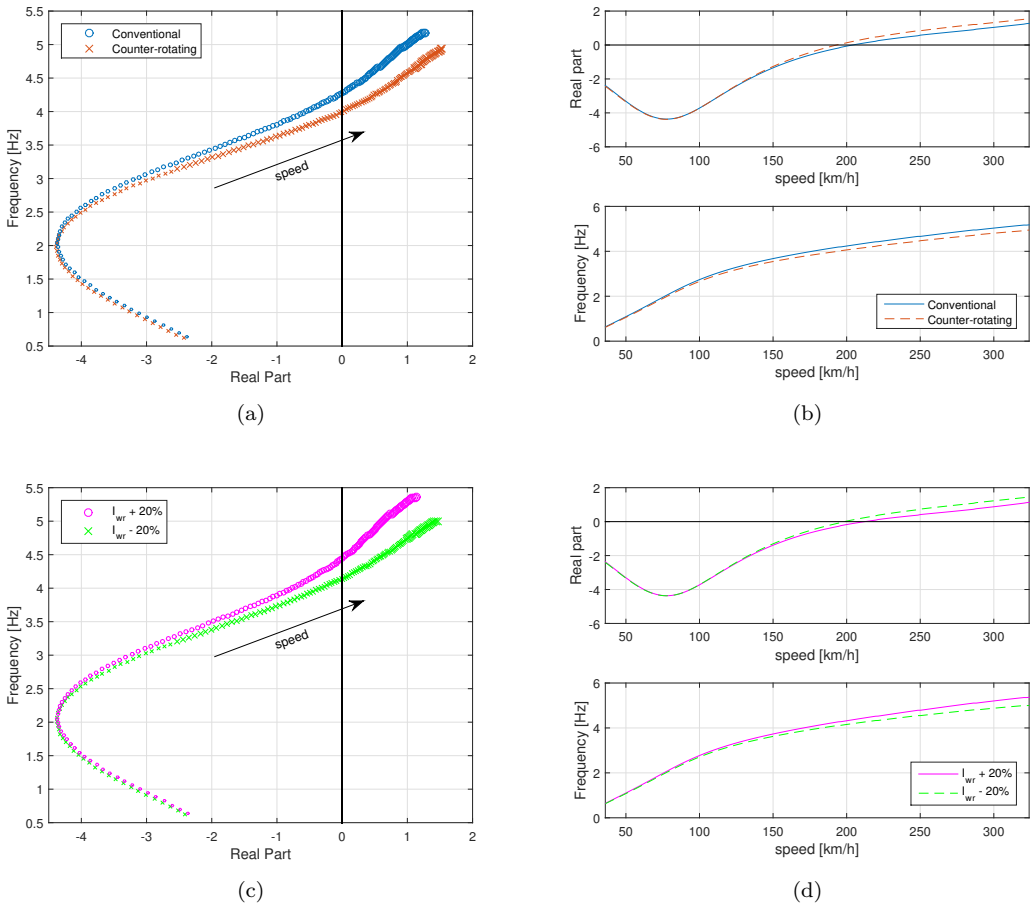

Figure 5.: Weave mode for speeds in the range 36-324 km/h: root-locus (a) and real part and frequency as a function of the vehicle speed (b) of the conventional engine vs. counter-rotating engine; root-locus (c) and real part and frequency as a function of the vehicle speed (d) of the conventional engine with rear wheel spin inertia $I_{wr} \pm 20\%$.

first variation of the unconstrained problem a boundary value problem is obtained. A finite difference discretisation yields to a large nonlinear system of algebraic equations which is solved using a root finding algorithm. Details on the solver are reported in [16].

6.1. *Acceleration*

The acceleration manoeuvre consists in completing a 500 m straight road in the minimum time, starting from an initial speed of 36 km/h.The manoeuvre is performed both with the conventional and counter-rotating engine, both on dry and wet conditions. In wet conditions the tyre-road friction coefficient is reduced by 33% with respect to the dry condition; Tab. 2.

It is preliminary noted that the maximum acceleration of the vehicle at the limit of wheelie (where the front tyre load is zero) is $b/h = 1.05\,\mathrm{g}$, while the maximum acceleration related to friction in dry condition is $\mu_{xr}^{dry} = 1.2\,\mathrm{g}$ [1]. Therefore, the maximum acceleration performance of the vehicle is limited by wheelie in dry condition, at least at low speeds, where the engine power is sufficient to reach the wheelie limit.

The results in dry conditions are reported in Fig. 6. The speed profiles of the two

configurations are very similar, Fig. 6a, however the counter-rotating configuration is slightly faster (9.901 s) than the conventional configuration (9.916 s), with a maximum speed difference of 0.5 km/h after 300 m. Fig. 6b highlights that both configurations are at the limits of wheelie for the first 300 m, since the engine torque delivered at the rear wheel (about 800 Nm) is lower than the available torque. The configuration with the counter-rotating engine is able to deliver slightly more torque, with a maximum difference around 4 Nm during the first 150 m. The advantage is built-up mainly in the first 300 m, where the gain is 0.012 s. The manoeuvre time difference at the end is 0.015 s.

As explained in the introduction, the advantage of the counter-rotating configuration in acceleration is a result of the reduced load transfer at the rear wheel for a given engine torque. When solving equation (4) with $N_f = 0$, the limit acceleration a_x with the two engine configurations is obtained

$$a_x = \frac{mgb - F_d h_a}{mh + I_{wr}/R_r + I_{wf}/R_f \pm I_e \tau_p \tau_g \tau_f / R_r}, \tag{31}$$

where the wheels angular accelerations $\dot{\omega}_r, \dot{\omega}_f$ and the engine angular acceleration $\dot{\omega}_e$ have been expressed as a function of a_x using the velocity ratios $1/R_r$, $1/R_f$ and $\tau_p\tau_g\tau_f/R_r$ respectively. Neglecting the aerodynamic drag force for simplicity, this expression gives an acceleration difference between the two configurations of 0.6% (first gear) and 0.3% (sixth gear). The numerical simulation of the dynamic model gives differences of 0.6% in first gear and 0.3% in third gear, while in taller gears the acceleration is no more limited by wheeling, but by the engine power.

Results in wet conditions are reported in Fig. 7. In wet condition the maximum acceleration related to friction is $\mu_{xr}^{wet} = 0.8$, which is lower than the maximum acceleration related to wheelie. In this scenario load transfer is beneficial and the conventional engine is expected to perform better. Fig. 7a shows that the speed profiles are again very similar, and the conventional engine is always slightly faster (12.052 s vs. 12.067 s), with a maximum speed difference of 0.3 km/h. Fig. 7b highlights that normal load on the rear wheel of the conventional configuration is always slightly larger than the normal load of the counter-rotating configuration, with a maximum difference around 7 N (equation (5) predicts an increase in the rear normal load of 5 N for the theoretical limit acceleration of 0.8 g, again assuming no drag for simplicity). Under wet condition, the advantage of the conventional configuration is 0.015 s.

6.2. *Braking*

The braking manoeuvre consists in slowing down the vehicle from the speed of 300 km/h to 36 km/h in the minimum time. As in the acceleration case, the manoeuvre is performed both with the conventional and counter-rotating engine, both in dry and wet conditions. As in the case of acceleration, in wet conditions the tyre-road friction coefficient is reduced by one third.

It is preliminary noted that the maximum deceleration of the vehicle at the limit of stoppie (where the rear tyre load is zero) is $(w - b)/h = 1.12$ g while the friction limit is dry condition is $\mu_{xr}^{dry} = 1.2$ [1]. As a consequence, the limit on the braking performance in dry condition is set by the stoppie limit. Results in dry condition are reported in Fig. 8. Both configuration start at the same speed of 300 km/h and are constrained to brake to 36 km/h in the minimum time. It is assumed that the engine remains engaged during the braking manoeuvre. In addition, because of the optimal control approach used, the (front to rear) braking ratio needs not to be predefined, since it is a result of the optimization.

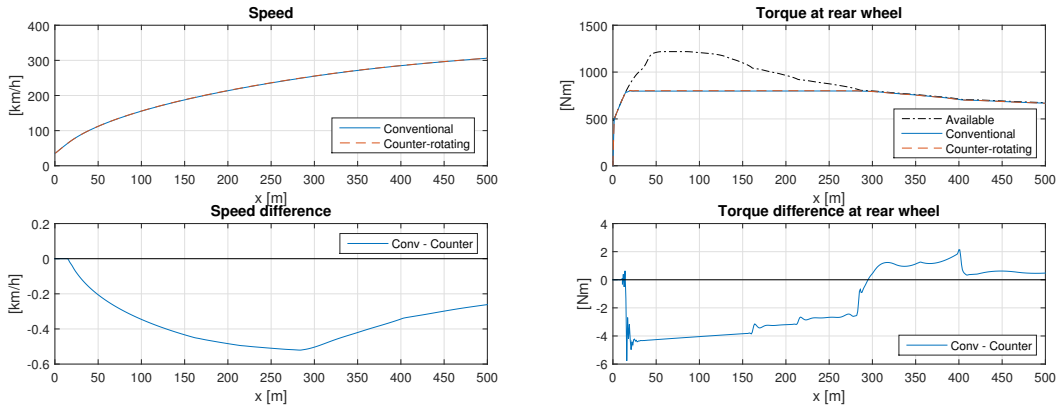

(a) (b)

Figure 6.: Acceleration in dry conditions: speed profile (a) and engine torque delivered at the rear wheel (b) as a function of the travelled distance.

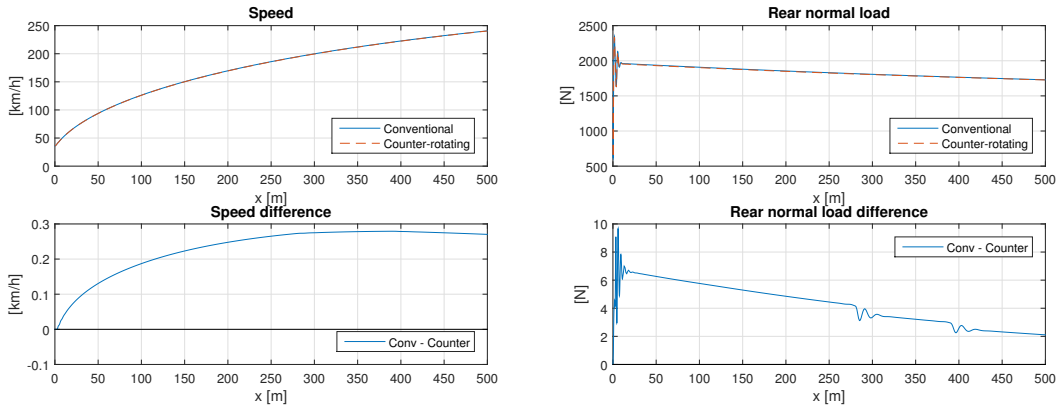

(a) (b)

Figure 7.: Acceleration in wet conditions: speed profile (a) and rear tyre normal load (b) as a function of the travelled distance.

Fig. 8a shows that in dry conditions the counter-rotating configuration brakes in 297.8 m (6.569 s) while the conventional configuration brakes in 299.0 m (6.600 s). The advantage of the counter-rotating configuration (1.2 m and 0.031 s) is again related to the reduced load transfer for a given longitudinal deceleration. As shown in Fig. 8b, the counter-rotating engine allows to use a greater front tyre longitudinal force to slow down the vehicle. The rear tyre longitudinal force is nearly zero for most of the manoeuvre, since the vehicle is braking at the stoppie limit. Similarly to the case of acceleration, equation (5) can be solved for $N_r = 0$ to give the limit deceleration

$$a_x = -\frac{mg(w-b) + F_d h_a}{mh + I_{wr}/R_r + I_{wf}/R_f \pm I_e \tau_p \tau_g \tau_f / R_r}. \tag{32}$$

Neglecting the aerodynamic forces for simplicity, the expression gives again an acceleration difference of 0.6% (first gear) and 0.3% (sixth gear). The numerical simulation of the dynamic model gives differences in the range 0.5-0.2%.

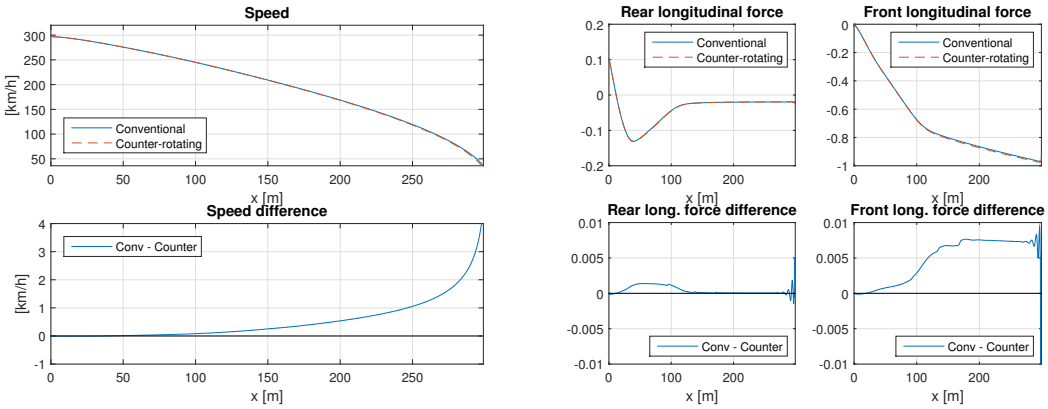

(a) (b)

Figure 8.: Braking from 300 to 36 km/h in dry conditions: speed (a) and longitudinal tyre forces per unit vehicle weight (b) as a function of the travelled distance.

In wet conditions, the friction limit reduces to $\mu_{xr}^{wet} = 0.8$, which is lower than the stoppie limit of the specific vehicle herein used. Therefore, when braking in wet conditions, as long as the front and rear tyre are engaged optimally, i.e. at their friction limits, the conventional and counter-rotating configurations give the same manoeuvre time (7.620 s) and braking distance (332.5 m). It is worth stressing the difference with respect to the acceleration case, where only one tyre is used for propulsion and thus increasing the load transfer is beneficial on low friction conditions, namely when the friction limit is lower than the wheelie limit.

7. Handling: lane-change

After the steady state analysis of section 4, the stability analysis of section 5 and the performance analysis of section 6, the focus will now move to the effect of engine layout on the handling of motorcycles. Similarly to the previous sections, methods and analysis will follow.

Lane-change tests are often used for the assessment of motorcycle handling. Therefore the effect of the engine layout on handling is herein quantified through a constant speed lane-change manoeuvre and the computation of the related Lane-Change-Roll-Index [17]

$$LCRI = \frac{\tau_{p-p}}{\dot{\phi}_{p-p} V}, \tag{33}$$

where τ_{p-p} is the peak-to-peak steering torque, $\dot{\phi}_{p-p}$ is the peak-to-peak roll rate and V is the average speed during the manoeuvre. A 3x21 lane-change is considered, which involves a lateral shift of 3 m over a transition distance of 21 m. The whole manoeuvre consists in riding straight for 30 m, performing the 3 m lateral shift in 21 m and completing the manoeuvre riding straight up to the end of the track at 80 m. The manoeuvre is obtained as the result of a minimum time problem when introducing the path constraints shown with dotted lines in Fig. 9. The lateral deviations with respect to the road centre line in the first 30 m (initial straight section) and the last 29 m (final straight section) is constrained to be in the range ± 0.050 m, while between 30 and 51 m (transition phase section) the lateral deviation is up to 3 m. In other words, the vehicle is constrained to

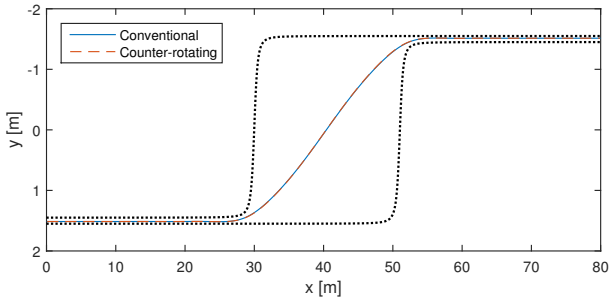

Figure 9.: Lane-change 3x21: trajectories at 90 km/h are depicted with solid and dashed lines while dotted lines represent the boundaries of the optimal control problem.

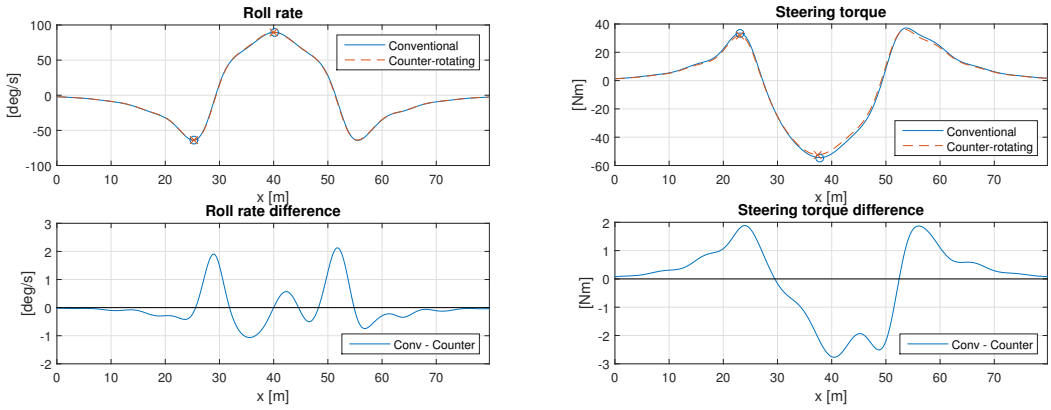

(a) (b)

Figure 10.: Roll rate (a) and steering torque (b) as a function of the travelled distance in a 3x21 lane-change at 90 km/h. Markers identify the peak values used for the computation of the LCRI.

go straight in the initial and final sections, while is free to take the preferred path in the transition section. The constant speed is enforced by an additional constraint on the maximum speed, which is set to the desired (constant) value.

Fig. 10 shows a 3x21 lane change at a speed of 90 km/h in terms of the roll rate and steering torque, which are the two signals necessary for the computation of the LCRI, together with the (constant) speed. The main differences are in the steering torque, where the counter-rotating engine has a smaller peak when beginning the lane-change (around 25 m of travelled distance), when changing the lean direction (around 35 m) and when exiting the lane-change (around 55 m). The result is that the LCRI of the counter-rotating engine is smaller than the LCRI of the conventional engine, namely 1.26 vs. 1.31. The counter-rotating configuration would therefore feel slightly 'lighter' and more responsive, which is consistent with experimental evidence. Results at 70, 80, 90 and 100 km/h are summarized in Tab. 1 and confirm the trend described in Fig. 10. It is also noted that the LCRI is almost speed-independent: this should not surprise since it is one of the reasons why such index was introduced [17].

Table 1.: LCRI for a 3x21 lane-change at different speeds.

Speed [km/h]	Conventional	Counter-rotating	Difference
70	1.314	1.258	4.2 %
80	1.314	1.258	4.3 %
90	1.312	1.255	4.3 %
100	1.311	1.251	4.5 %

8. Conclusion

The work has addressed the effect of the engine spin direction on the dynamics of motorcycles. The analysis started from simple formulae that uncover the basic effects of engine layout on the dynamics of single track vehicles. Then the numerical analysis of a detailed motorcycle model has been presented in order to quantify the effects predicted by the theory. The model has been studied in terms of its equilibria, vibration modes, acceleration/braking performance and handling characteristics. A minimum time manoeuvring approach has been used to asses the limit performance of the vehicle and the handling behaviour. It was found that, when compared to the conventional configuration, the counter-rotating configuration has a smaller equilibrium roll angle (0.2-0.4% in the model analysed – the shorter the engaged gear, the higher the difference), less stable weave mode (up to 0.5% in the real part at maximum speed, in the model analysed), better acceleration performance in dry conditions (when the maximum acceleration is limited by wheelie; up to 0.6% increase in the limit acceleration in the model analysed) and better lane-change performance (up to 4.5% reduction in the Lane-Change-Roll-Index in the model analysed).

References

[1] Cossalter V. Motorcycle dynamics. Lulu; 2006.
[2] Sharp RS. Motorcycle steering control by road preview. Journal of Dynamic Systems, Measurement and Control, Transactions of the ASME. 2007;129(4):373–381.
[3] Sharp RS. Optimal preview speed-tracking control for motorcycles. Multibody System Dynamics. 2007;18(3):397–411.
[4] Rowell S, Popov AA, Meijaard JP. Application of predictive control strategies to the motorcycle riding task. Vehicle System Dynamics. 2008;46(S1):805–814.
[5] Massaro M. A nonlinear virtual rider for motorcycles. Vehicle System Dynamics. 2011;49(9):1477–1496.
[6] Saccon A, Hauser J, Beghi A. A virtual rider for motorcycles: Maneuver regulation of a multi-body vehicle model. IEEE Transactions on Control Systems Technology. 2013;21(2):332–346.
[7] Cossalter V, Da Lio M, Lot R, Fabbri L. A general method for the evaluation of vehicle manoeuvrability with special emphasis on motorcycles. Vehicle System Dynamics. 1999;31:113–135.
[8] Bobbo S, Cossalter V, Massaro M, Peretto M. Application of the optimal maneuver method for enhancing racing motorcycle performance. SAE International Journal of Passenger Cars-Mechanical Systems. 2009;1(1):1311–1318.
[9] Tavernini D, Massaro M, Velenis E, Katzourakis D, Lot R. Minimum time cornering: The effect of road surface and car transmission layout. Vehicle System Dynamics. 2013;51(10):1533–1547.
[10] Perantoni G, Limebeer DJN. Optimal control of a formula one car with variable parameters. Vehicle Systems Dynamics. 2014;52(5):653–678.
[11] Tremlett AJ, Limebeer DJN. Optimal tyre usage on a formula one car. Vehicle System Dynamics. 2016;54(10):1448–1473.
[12] Pacejka HB. Tire and vehicle dynamics. 3rd ed. Butterworth-Heinemann; 2012.
[13] Sharp RS, Evangelou S, Limebeer DJN. Advances in the modelling of motorcycle dynamics. Multibody System Dynamics. 2004;12(3):251–283.

[14] Cossalter V, Lot R, Massaro M. An advanced multibody code for handling and stability analysis of motorcycles. Meccanica. 2011;46(5):943–958.
[15] Tremlett AJ, Massaro M, Purdy DJ, Velenis E, Assadian F, Moore AP, Halley M. Optimal control of motorsport differentials. Vehicle System Dynamics. 2015;53(12):1772–1794.
[16] Bertolazzi E, Biral F, Da Lio M. Symbolic-numeric efficient solution of optimal control problems for multibody systems. Journal of computational and applied mathematics. 2006;185(2):404–421.
[17] Cossalter V, Sadauckas J. Elaboration and quantitative assessment of manoeuvrability for motorcycle lane change. Vehicle System Dynamics. 2006;44(12):903–920.

9. Appendix

Table 2.: Bike (plus rider) parameters.

Symbol	Description	Value
	Vehicle plus rider	
m	Vehicle mass	250 kg
h	Height of centre of mass	0.69 m
b	Longitudinal distance of centre of mass from rear axle	0.73 m
w	Wheelbase	1.5 m
a_n	Normal trail	0.1 m
ε	Caster angle	0.45 rad
I_x	Moment of inertia about the x-axis	18 kg m^2
I_y	Moment of inertia about the y-axis	50 kg m^2
I_z	Moment of inertia about the z-axis	40 kg m^2
I_{xy}	Product of inertia ($I_{xz} = \int xzdm$)	-2 kg m^2
C_dA	Drag area coefficient (acceleration)	0.2 m^2
C_dA	Drag area coefficient (deceleration)	0.5 m^2
C_lA	Lift coefficient	0.05 m^2
h_a	Height of aerodynamic centre of pressure	0.51 m
	Front frame	
m_f	Front frame mass	30 kg
h_f	Height of mass centre	0.55 m
b_f	Longitudinal distance of mass centre from rear axle	1.36 m
I_{fz}	Moment of inertia about the z-axis (steer)	0.48 kg m^2
	Rear wheel and tyre	
m_{ur}	Unsprung mass	25 kg
I_{wr}	Spin inertia	0.67 kg m^2
R_r	Tyre radius	0.33 m
t_r	Tyre crown section radius	0.10 m
k_{pr}	Tyre radial stiffness	154 kN/m
c_{pr}	Tyre radial damping	200 Ns/m
$k_{\lambda r}$	Sideslip stiffness per unit load	15 rad^{-1}
$k_{\phi r}$	Roll stiffness per unit load	0.8 rad^{-1}
σ_r	Relaxation length	0.15 m
μ_{xr}^{dry}	Longitudinal friction coefficient on dry tarmac	1.2
μ_{yr}^{dry}	Lateral friction coefficient on dry tarmac	1.4
μ_{xr}^{wet}	Longitudinal friction coefficient on wet tarmac	0.8
μ_{yr}^{wet}	Lateral friction coefficient on wet tarmac	0.9
	Front wheel and tyre	
m_{uf}	Unsprung mass	11 kg
I_{wf}	Spin inertia	0.41 kg m^2
R_f	Tyre radius	0.30 m
t_f	Tyre crown section radius	0.06 m
k_{pf}	Tyre radial stiffness	157 kN/m
c_{pf}	Tyre radial damping	200 Ns/m
$k_{\lambda f}$	Sideslip stiffness per unit load	13 rad^{-1}
$k_{\phi f}$	Roll stiffness per unit load	0.9 rad^{-1}
σ_f	Relaxation length	0.12 m
μ_{xf}^{dry}	Longitudinal friction coefficient on dry tarmac	1.2
μ_{yf}^{dry}	Lateral friction coefficient on dry tarmac	1.4
μ_{xf}^{wet}	Longitudinal friction coefficient on wet tarmac	0.8
μ_{yf}^{wet}	Lateral friction coefficient on wet tarmac	0.9

Table 3.: Bike (plus rider) parameters (cont.).

Symbol	Description	Value
	Engine and transmission	
I_e	Engine spin inertia	$0.016\,\mathrm{kg\,m^2}$
τ_p	Primary ratio	1.559
τ_{g1}	1st gear	2.429
τ_{g2}	2nd gear	2.133
τ_{g3}	3rd gear	1.889
τ_{g4}	4th gear	1.647
τ_{g5}	5th gear	1.450
τ_{g6}	6th gear	1.316
τ_f	Final ratio	2.750
	Suspensions	
k_r	Rear suspension rotational stiffness	$30000\,\mathrm{N/m}$
c_r	Rear suspension rotational damping	$1500\,\mathrm{Ns/m}$
k_f	Front suspension linear stiffness	$25\,\mathrm{kN/m}$
c_f	Front suspension damping	$1\,\mathrm{kNs/m}$
	Contraints	
P_{max}	Engine maximum power	$200\,\mathrm{kW}$
$\delta_{\max}$	Maximum steering angle	$0.2\,\mathrm{rad}$
$T_{\max}$	Maximum handlebar torque	$160\,\mathrm{Nm}$
$n_{\max}$	Maximum road half-width	$1.5\,\mathrm{m}$

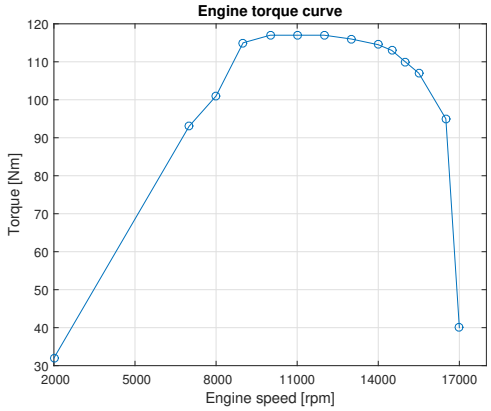

Figure 11.: Engine torque curve.